Uncertainties in the Radiative Forcing Due to Sulfate Aerosols

GUNNAR MYHRE,* FRODE STORDAL,* TORE F. BERGLEN, JOSTEIN K. SUNDET, AND IVAR S. A. ISAKSEN

Department of Geophysics, University of Oslo, Oslo, Norway

(Manuscript received 8 August 2002, in final form 29 November 2002)

ABSTRACT

Radiative transfer calculations based on a new sulfate distribution from a chemistry-transport model simulation have been performed. A wide range of sensitivity experiments have been performed to illustrate the large uncertainty in the radiative forcing due to sulfate aerosols. The most important factors seem to be processes involved in the mixing of sulfate aerosols with other particles and uncertainties in the relative humidities. These factors can explain much of the large range in previous estimates of the radiative forcing due to sulfate aerosols reflected, for example, in the Intergovernmental Panel on Climate Change estimate. Included in this study is a simple subgrid-scale parameterization of relative humidity to investigate a potentially large uncertainty in the radiative forcing due to sulfate aerosol.

1. Introduction

Several global studies of the direct effect of sulfate aerosols have been performed with large differences in the estimates of the radiative forcing (Myhre et al. 1998; Haywood and Boucher 2000; Adams et al. 2001; Houghton et al. 2001). In addition to uncertainties in the global burden of sulfate, uncertainties in the forcing have several causes. First, there are uncertainties connected to the optical properties of sulfate aerosols. The optical properties adopted in the global simulations are often calculated with Mie theory. In Mie theory, size and refractive index are used along with the assumption of spherical particles. In particular the size distribution of sulfate aerosols is uncertain. The size of the sulfate aerosols is connected to their mixing with other aerosols, which can also alter the refractive index.

The hygroscopicity of the sulfate aerosols introduces several uncertainties. It has been taken into account in many different ways in earlier studies by adoption of different parameterizations. Further, the relative humidity varies substantially in different global models. In addition, Haywood et al. (1997a) and Myhre et al. (2002) show that subgrid-scale variation in relative humidity is important and that global models underestimate the magnitude of the radiative forcing of the hygroscopic aerosols. Clouds reduce the magnitude of the radiative forcing due to scattering aerosols. The relative humidity is generally high in regions with clouds, connecting the importance of relative humidity and clouds. Houghton et al. (2001) states that these two factors are the major causes of the large spread in earlier global studies.

The spatial distribution of sulfate is also important as the radiative forcing due to sulfate depends on relative humidity, surface albedo, and clouds, which all have a spatial pattern.

Over the last years, observational campaigns, such as, the Tropospheric Aerosol Radiative Forcing Observational Experiment (TARFOX), the first and second Aerosol Characterization Experiments (ACE-1 and ACE-2), the Indian Ocean Experiment (INDOEX), and the Southern African Regional Science Initiative (SAFARI-2000), have given useful insight into physical and chemical characteristics of aerosols. Future campaigns connected to long-term ground-based and satellite remotely sensed aerosol are necessary to improve the knowledge and confidence in estimates of radiative forcing due to aerosols.

In this study we use a new sulfate distribution and investigate several effects of importance for the radiative forcing due to sulfate aerosols. We start by using several sulfate distributions and several different assumptions on optical properties of sulfate aerosols. Furthermore, we elaborate on uncertainties due to relative humidity and clouds by adopting data from various sources.

2. Models

a. Chemistry transport modeling of the sulfate distribution

The global sulfate distribution is calculated using the Oslo chemical transport model 2 (CTM2; T. Berglen et

* Additional affiliation: Norwegian Institute for Air Research, Kjeller, Norway.

Corresponding author address: Dr. Gunnar Myhre, Department of Geophysics, University of Oslo, P.O. Box 1022, Blindern, Oslo 0315, Norway.
E-mail: gunnar.myhre@geofysikk.uio.no

al. 2003, manuscript submitted to *J. Geophys. Res.*, hereafter BER). The model is run in a T21 (5.6° × 5.6°) resolution, with 19 vertical levels from the surface to 10 hPa, and a vertical resolution of approximately 1 km in the troposphere. The model uses offline precalculated meteorological and physical data for 1996 from the European Centre for Medium-Range Weather Forecasts (ECMWF). Advection adopts the second-order moment scheme (Prather 1986). Convection uses mass flux data from the ECMWF convective parameterization (Tiedtke 1989) and is based on the surplus or deficit of mass in a column. Boundary layer turbulence is estimated using the Holtslag K-profile boundary layer scheme (Holtslag et al. 1990). Three-dimensional rainfall (from the precalculated meteorological data) is used to estimate the wet removal of hygroscopic tracers, both for large-scale removal and in convective events. The model calculates the global distribution of chemical compounds using an extensive chemical scheme, which includes chemical compounds in the oxygen, hydrogen, nitrogen, carbon, and sulfur families. In particular calculation of SO_2 conversion to sulfate is coupled to calculations of chemical compounds like OH, H_2O_2, and O_3, and to removal of sulfur compounds through dry deposition and precipitation events. The quasi-steady-state approximation integrator (Hesstvedt et al. 1978; Berntsen and Isaksen 1997) is used to solve chemical equations. During the beginning of the 1990s there were significant changes in the emission patterns of sulfur compounds, with reduced emissions over the United States and Europe and significant increases in emissions over Southeast Asia. Sulfur emissions from antropogenic sources representative for 1985 as well as 1996 have been adopted in the model studies (BER).

While the distribution of the primary compound SO_2 closely resembles the distribution in anthropogenic emissions, with high levels over polluted regions in the Northern Hemisphere, due to its short lifetime (approximately 1–2 days), the sulfate is distributed over larger horizontal and vertical regions. This is partly due to sulfate being a secondary compound, and partly due to its longer atmospheric lifetime (3–4 days). High sulfate levels are often found over and downstream of Northern Hemispheric industrial continents, especially Europe, southeastern United States, and eastern Asia. Although there is a significant transport of sulfate out of continents, the sulfate burden is typically one order of magnitude lower over oceanic regions than over the continents in the Northern Hemisphere. The calculated burden is significantly higher during summer months than during winter months at northern latitudes due to more efficient oxidation of SO_2 to sulfate. The sulfate burden based on anthropogenic emission for 1996 show a decease over Europe and the United States (45% and 20%, respectively) and a significant increase over eastern Asia (80%) compared to 1985.

b. Radiative transfer modeling

For the radiative transfer calculations of solar radiation we apply a multistream model using the discrete-ordinate method (Stamnes et al. 1988). In the radiative transfer calculations, eight streams are used. Rayleigh scattering and clouds are included in the radiative transfer model, and the exponential sum-fitting method (Wiscombe and Evans 1977) is used to account for absorption by gases (see Myhre et al. 2002 for further details).

Our reference calculations are performed with T21 spatial resolution (about 5.6° × 5.6°) and 19 vertical layers, but another spatial resolution is also investigated. Global distribution of temperature, water vapor, clouds, and surface albedo, at a 3-h time resolution, is adopted from the ECMWF for the year 1996.

The random cloud overlap assumption is adopted, based on radar observations (Hogan and Illingworth 2000). The optical properties of clouds are calculated using the procedure described in Slingo (1989) with effective radius of 10 μm for low clouds (Stephens and Platt 1987) and 18 μm for high clouds. No sulfate aerosol cloud interaction is considered in this study.

c. Optical properties

The optical properties (specific extinction coefficient, single scattering albedo, and asymmetry factor) used in this study for dry aerosols and for wet aerosols at relative humidities above 30% are the same as in Myhre et al. (1998), where the growth of the aerosols for relative humidities above 81% was based on Fitzgerald (1975). A lognormal size distribution is used with geometric mean radius (r_m) of 0.05 μm with a geometric standard deviation (σ) of 2.0. The refractive index for ammonium sulfate is adopted from Toon et al. (1976).

3. Radiative forcing

Table 1 shows a list of experiments that are performed. Starting from reference calculation (1985 emission) in which treatment of processes and parameterizations are described above, we have performed several sensitivity experiments investigating different sulfate distributions, factors affecting the optical properties of sulfate, and uncertainties in meteorological data. Table 2 shows the global and annual mean results of the radiative forcing calculations.

a. Reference calculation

In the reference calculation a global and annual mean radiative forcing of -0.37 W m^{-2} (-0.67 W m^{-2} for clear sky) is calculated and the global distribution is shown in Fig. 1a. The global and annual mean aerosol optical depth (AOD) at 500 nm is 0.019 with maximum of 0.39 over a small region in Asia and with generally larger regions in Europe and North America with AOD

TABLE 1. Description of calculations.

Issue	Description
Reference	Standard optical properties and a T21 resolution
Sulfate distribution	Change in emissions and data from another model
Size distribution	Use of other observed size distributions
Refractive index	Refractive index for other sulfate components
Internal mixing	Mixing with other aerosol components
Growth factor	Different treatment of the hygroscopic sulfate aerosols
Phase function	Calculation with Mie phase function
Spatial resolution	Calculation for higher spatial resolution
Relative humidity	Data for relative humidity from various sources
Clouds	Satellite data for clouds
Surface albedo	Calculation of surface albedo from another source
Subgrid relative humidity	Parameterization of relative humidity for higher spatial resolutions

above 0.3. The atmospheric anthropogenic aerosol burden of sulfate (1.79 mg m^{-2}) is somewhat lower than the burden of the water associated with the sulfate aerosols (2.20 mg m^{-2}). The normalized radiative forcing is -207 W g^{-1}. The Northern Hemisphere to Southern Hemisphere ratio in the radiative forcing is 4.6. The two last values are close to mean values of earlier estimates (Houghton et al. 2001). The relative humidity increases the radiative forcing with a factor of 1.34, which is slightly higher than in Myhre et al. (1998), but lower than in Haywood et al. (1997) and Boucher and Anderson (1995).

b. Sulfate distribution

Calculations with anthropogenic SO_2 emissions for 1996 instead of 1985 have been performed. Subsequent radiative forcing results are shown in Fig. 1b, showing a significant change in the geographical distribution with a shift in the forcing from northern America and Europe to Asia. However, the global mean forcing changes only modestly, with 7%, reflecting the change in the global mean sulfate burden. Therefore, the normalized radiative forcing is unchanged. The interhemispheric ratio in the forcing is reduced from 4.6 in the reference calculation to 3.7 in this simulation.

TABLE 2. Radiative forcing due to sulfate (see text for further explanation). W78 refers to Withby (1978); Q95 to Quinn et al. (1995), W99 to Weingartner (1999), and CH93 to Covert and Heintzenberg (1993).

Issue	Description	Radiative forcing (W m^{-2})
Reference		−0.37
Sulfate distribution	1996 emission	−0.40
	Langner and Rodhe (1991)	−0.38
Size distribution	Accumulation mode (CH93 (see Fig. 2)	−0.41
	Accumulation mode (Q95)	−0.39
	Accumulation mode (W99)	−0.38
	Accumulation mode (W78)	−0.35
	Three mode (Q95)*	−0.21
	Three mode (Q95)*	−0.15
Refractive index	Sulfuric acid	−0.30
Internal mixing	Soot with volume mixing rule	−0.06
	Soot with Maxwell–Garnett mixing rule	−0.09
	Sea salt**	−0.28
	Mineral dust**	−0.30
Growth factor	Köhler equation	−0.38
Phase function	Mie phase function	−0.37
Spatial resolution	T63 resolution	−0.39
Subgrid relative humidity	Representation of T63 resolution	−0.39
	Representation of 50-km resolution	−0.42
Surface albedo	Solar and spectral dependence included	−0.39
Clouds	ISCCP clouds	−0.43
Relative humidity	NCAR	−0.60
	NCEP	−0.38
	GFDL	−0.47
	GISS	−0.46

* Calculation based on data from two different campaigns.
** Calculation based on 4 days with a radiative forcing similar to the reference calculation.

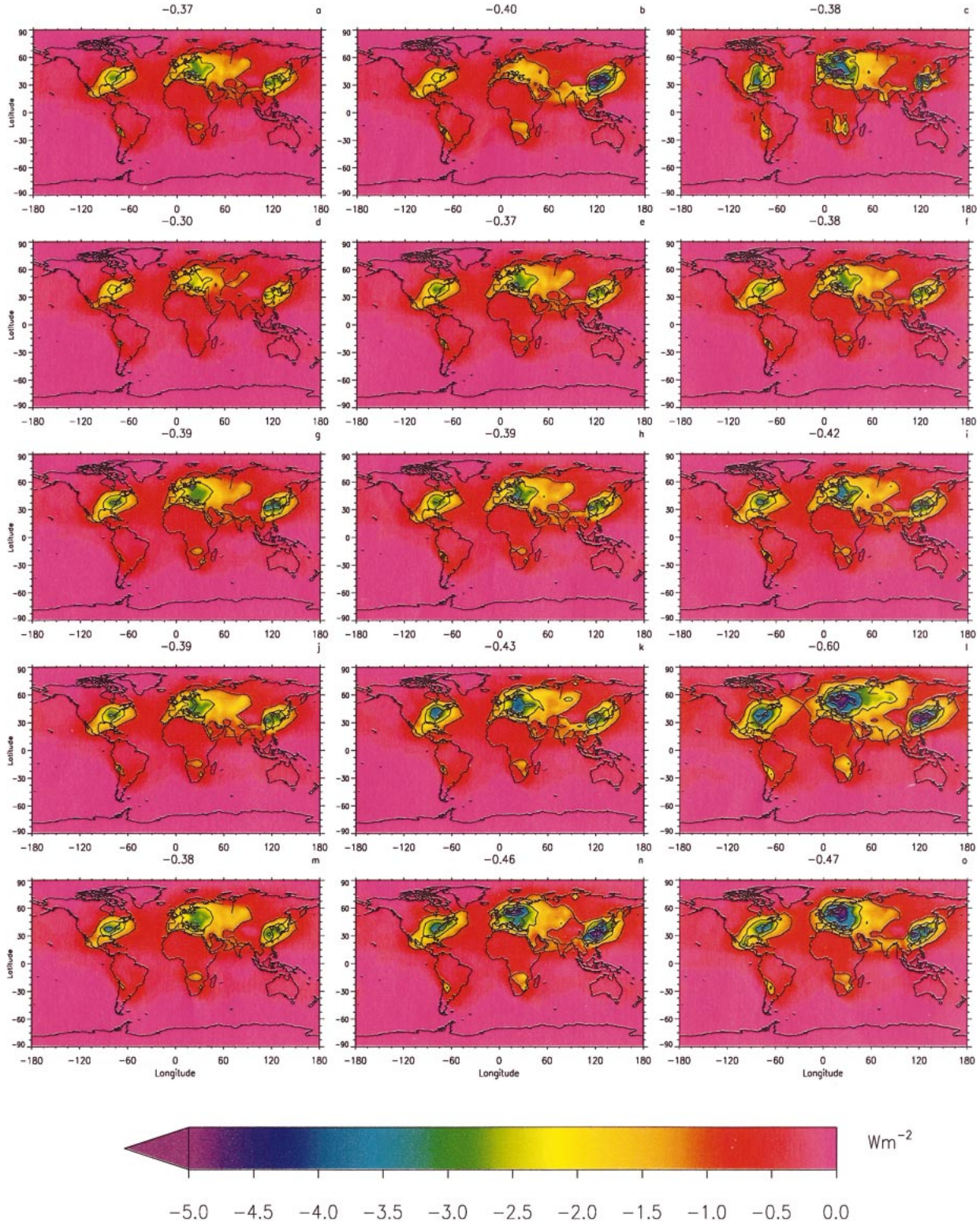

FIG. 1. Radiative forcing due to anthropogenic sulfate: (a) reference case, (b) emission data for 1996, (c) Langner and Rodhe (1991) sulfate data, (d) refractive index of sulfuric acid, (e) full phase function, (f) growth according to the Köhler equation, (g) T63 resolution for meteorological data (see text), (h) subgrid parameterization of relative humidity for T63, (i) subgrid parameterization of relative humidity for 50-km resolution, (j) spectral and solar zenith angle dependence of surface albedo, (k) cloud data from ISCCP, (l) relative humidities from NCAR CCM3, (m) relative humidities from NCEP, (n) relative humidities from GISS GCM, and (o) relative humidities from GFDL GCM.

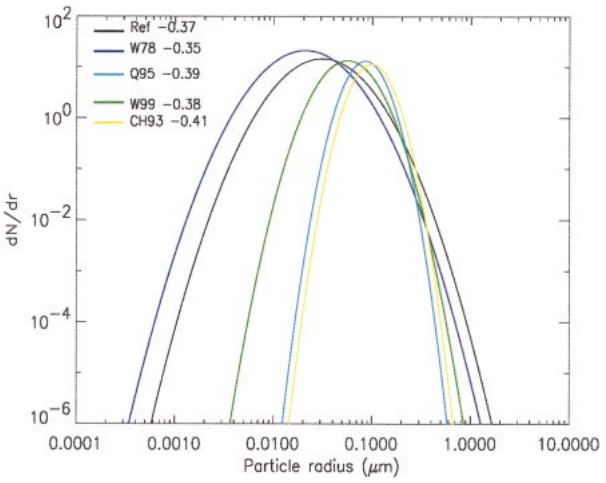

FIG. 2. Size distribution used in the reference calculation and some observations of the accumulation mode. W78 refers to Withby (1978), Q95 to Quinn et al. (1995), W99 to Weingartner et al. (1999), CH93 to Covert and Heintzenberg (1993).

The sulfate distribution from the fast oxidation case from Langner and Rodhe (1991) has been used in a radiative forcing calculation. The geographical distribution in the burden is more localized in the industrial regions in this dataset compared to the reference calculation, except in southern North America where the transport of sulfate over ocean is much larger than in the reference calculation. The anthropogenic sulfate burden of 1.90 mg m^{-2} is slightly higher than in the reference case used in this study. On the other hand, the sulfate burden is slightly lower than calculated in Charlson et al. (1991) based on the same Langner and Rodhe (1991) data, which is due to different pressure conversion of the data. The geographical distribution of the radiative forcing is shown in Fig. 1c. It is rather similar to the distribution in the reference calculation. The global and annual mean forcing is only 2% stronger than with the reference sulfate distribution. In the clear-sky simulation this difference is larger (13%). The normalized radiative forcing is -200 W g^{-1}, also modestly different from the reference simulation.

c. Optical properties

1) SIZE DISTRIBUTION

Based on various observations of the size distribution (as shown in Fig. 2) radiative forcing calculations are performed. Note that the size distribution from the observations is not necessarily for sulfate aerosols only, but they represent a range of accumulation size particles. The r_m ranges from 0.0345 to 0.11 μm and σ from 1.4 to 2.03 illustrating that uncertainties in the size distribution are significant. The range in the radiative forcing due to sulfate aerosols based on these size distributions is about 15%. Boucher and Anderson (1995) explored a wider range of size distributions and found a larger range related to this effect.

For size distributions including larger aerosols, mixing with other aerosols is important [see section 3c(6)]. Observations show that sulfate components are also included in size distributions with large particles. However, the fraction is often low; therefore size distributions including large particles represent the lower range of possible forcings. Observations over ocean (two campaigns in Quinn et al. 1995) yielded three-mode lognormal size distributions (including a coarse mode). These size distributions resulted in a radiative forcing between -0.15 and -0.21 W m^{-2}, highlighting size distributions and mixing with other aerosols as a major uncertainty in radiative forcing due to sulfate.

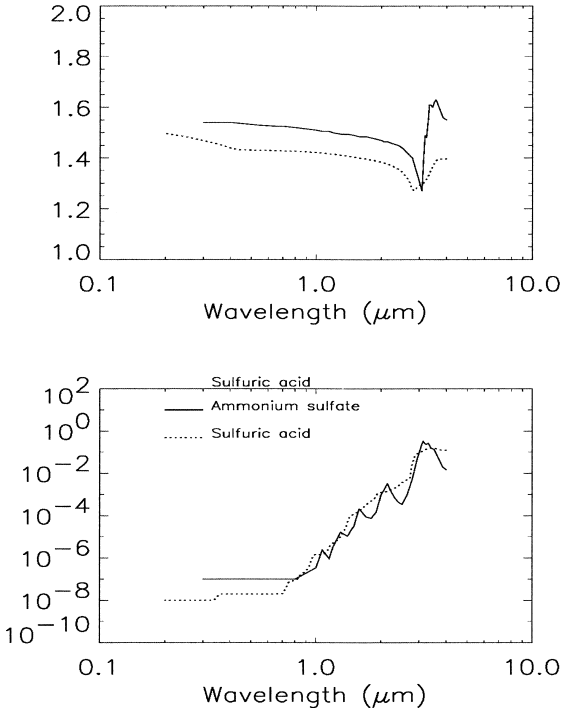

FIG. 3. Refractive index for ammonium sulfate (Toon et al. 1976) and 75% sulfuric acid (Palmer and Williams 1975). (top) Real and (bottom) imaginary refractive index.

2) REFRACTIVE INDEX

Figure 3 shows refractive index for ammonium sulfate (Toon et al. 1976) and sulfuric acid (Palmer and Williams 1975). Boucher and Anderson (1995) found that the radiative forcing assuming either ammonium sulfate or sulfuric acid aerosols made a small difference in the global and annual mean radiative forcing. This is due to a compensation between the stronger hygroscopicity and smaller refractive index for sulfuric acid compared to ammonium sulfate aerosols.

In a simulation using the refractive index of sulfuric acid (the only assumptions deviating from the reference

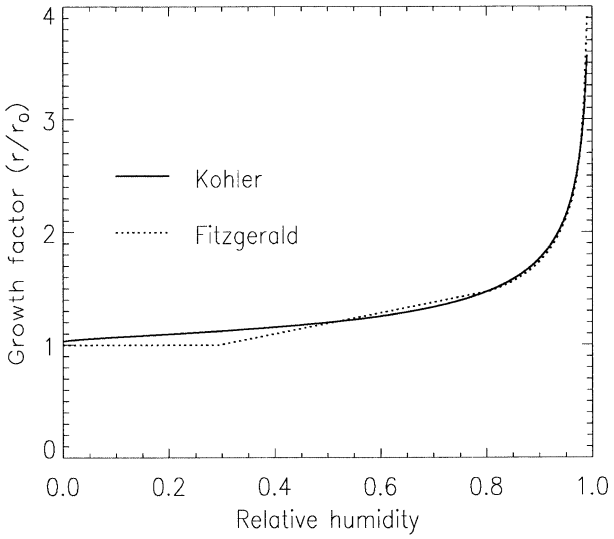

FIG. 4. Growth factor for sulfate aerosols at $r = 0.05$ μm based on Fitzgerald (1975) and the Köhler equation.

calculation) the radiative forcing is 20% lower than in the reference case. This demonstrates a large sensitivy to the refractive index and the importance of consistency between the choice of refractive index and the hygroscopic effect. Figure 1d shows the geographical distribution of the radiative forcing based on the sulfuric acid refractive index.

3) PHASE FUNCTION

Boucher (1998) found that using the full phase function instead of the Henyey–Greenstein phase function (which often is used in global calculations) could introduce differences up to 20% in the radiative forcing due to aerosols for different aerosol sizes and solar zenith angles. In global and annual mean calculations of the radiative forcing due to sulfate aerosols the difference between the two phase functions is less than 1% due to the large cancellation with solar zenith angle. Figure 1e shows the global distribution, yielding regional differences smaller than 5%.

4) GROWTH FACTOR

Figure 4 compares the hygroscopic growth based on the parameterization of Fitzgerald (1975) with the Köhler equation (see e.g., Pruppacher and Klett 1978). The figure shows the important hygroscopic growth for high relative humidities and that the differences between the two approaches are small. Note that the results shown in Fig. 4 are for dry aerosols with radius of 0.05 μm, but the results are rather similar for other radii. We estimate that the deviation in global mean radiative forcing between the two approaches is 2.5%, which is mainly due to differences in the growth factor below relative humidity of 81%. This is owing to the fact that, in the reference calculation, a linear growth in radius is assumed with relative humidity between 30% and 81%, whereas the Köhler equation is used for all relative humidities. A calculation where the Köhler equation is used only for relative humidities above the deliquescence point resulted in smaller than 1% deviation from the reference case in radiative forcing. Figure 1f shows the global distribution of the radiative forcing with hygroscopic growth adopting the Köhler equation. The distribution is very similar to the reference calculation with regional differences up 5%–10% with most efficient strengthening of the forcing over dry regions.

TABLE 3. Comparison of radiative forcing using T21 and T63 spatial resolutions for meteorological data.

	Clear dry	Clear	Clouds dry	Clouds
T21 (W m^{-2})	−0.43	−0.64	−0.28	−0.37
T63 (deviation from T21)	0%	12%	0%	5%

5) SPATIAL RESOLUTION AND SUBGRID-SCALE RELATIVE HUMIDITY

Haywood et al. (1997a) and Myhre et al. (2002) showed that subgrid-scale variability in global models tends to underestimate the magnitude of the forcing due to sulfate aerosols. This arises from averaging the relative humidity, since the hygroscopic growth is nonlinear, as can be seen from Fig. 4. Table 3 shows a comparison of the reference calculation (T21) with a calculation using the T63 (about $1.9° \times 1.9°$) spatial resolution of the ECMWF meteorological data such as relative humidity and clouds. The sulfate distribution is the same in both calculations (T21 resolution). Simulations are performed for clear sky and calculations including clouds in both cases for hygroscopic sulfate aerosols and dry aerosols (no hygroscopic growth). The results show that the radiative forcing due to sulfate aerosols is insensitive to spatial resolution for dry aerosols. However, significant deviations are found when humidity is taken into account. The impact of humidity is larger for clear sky than when clouds are included, as high relative humidity and clouds are often collocated and as clouds strongly reduce the forcing. The results are in accordance with the results found in Myhre et al. (2002) for a similar difference in spatial resolution in relative humidity. Ghan et al. (2001a) also found that the radiative forcing due to sulfate was dependent on the spatial resolution, but in their simulations also the sulfate burden was changed. Figure 1g shows the geographical distribution of the radiative forcing calculations with T63 meteorological data.

In an attempt to take into account the variability in relative humidity in global models, we have made a simple subgrid-scale parameterization. The spatial resolution in the T63 dataset is 3 times higher in longitudinal as well as latitudinal direction than in T21. With-

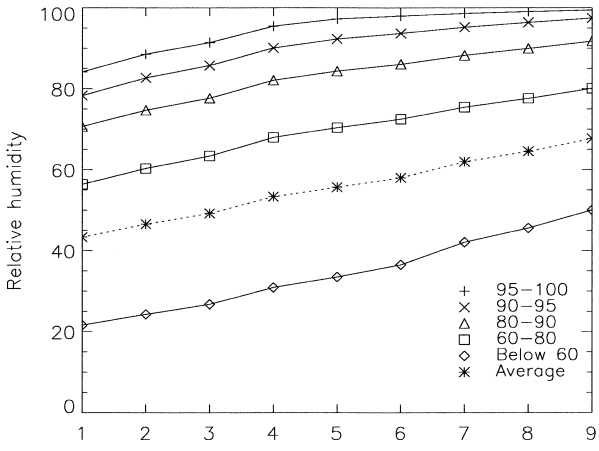

FIG. 5. Variation in relative humidity over nine grid points (three longitudinal and three latitudinal) over a T21 grid based on T63 data. The variation in relative humidity is grouped into five intervals and ordered in increasing values.

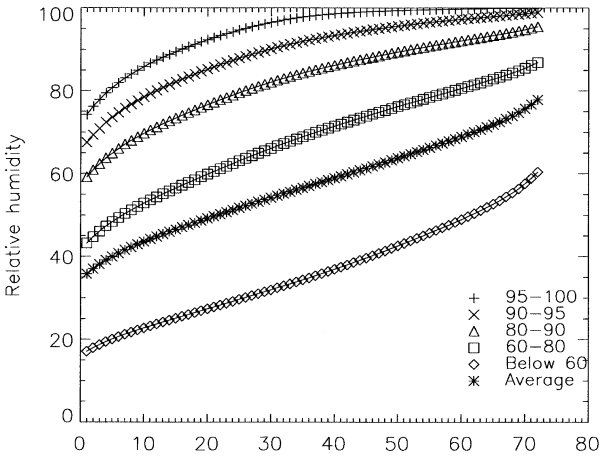

FIG. 6. Same as Fig. 5, but for a 50-km resolution and 72 grid points within the T21 resolution.

in one T21 grid cell there are thus nine cells in the T63 resolution. We have sorted the relative humidity data for the nine cells in ascending order in nine categories; thereafter, we have averaged the values in each category over all T21 cells globally. Finally, the data are sorted in five classes according to the level of relative humidity (in the T21 resolution). The globally averaged sorted dataset is shown in Fig. 5. The results cover the 10 lowest layers (about 8 km). The results show that the difference in relative humidity within a T21 grid (based on T63 data) decreases somewhat with increasing relative humidity. The variability in relative humidity shown in the figure is substantially around 20 relative humidity percentage units. We have included the variability found for the five intervals of relative humidity for global conditions into a T21 simulation, by adopting this variation in relative humidity for each T21 grid cell. The resulting global mean radiative forcing is within 1% of the regular T63 experiment. Also in this test of a subgrid-scale parameterization we find a larger effect when clouds are excluded than included in the calculations. In Fig. 1h, the geographical distribution of the forcing using this subgrid-scale parameterization is shown. In both Figs. 1g and 1h the strengthening of the forcing is mostly over ocean, but in the regular T63 calculations this is mostly localized to coastal regions, and in the subgrid-scale calculation, more generally over the ocean.

The results of Haywood et al. (1997a) and Myhre et al. (2002) showed that relative humidity variations is of importance for spatial resolutions higher than T63. Figure 6 shows variability in relative humidity based on 50-km relative humidity data from Myhre et al. (2002) within a T21 grid. The procedure for sorting the data is identical to the one described above, except that there are now 72 grid cells within each T21 cell. Note that this data presentation is based on the region studied in Myhre et al. (2002), namely, Europe, the North Atlantic, and part of North America, and it does not necessarily represent global conditions. The radiative forcing is strengthened by about 15% (slightly more for clear-sky condition) using the 50-km subgrid-scale variability in relative humidity compared to the reference calculation (T21). Figure 1i shows the geographical distribution of the forcing, exhibiting a strengthing of the radiative forcing by up to 25% regionally. The largest strengthening occurs in oceanic regions close to industrialized areas. Over Europe, Southeast Asia, and North America the strengthing in the radiative forcing is generally around 15%.

6) INTERNAL MIXING

Internal mixing of sulfate and soot is earlier shown to reduce the cooling effect of sulfate aerosols (Haywood et al. 1997b; Myhre et al. 1998). Jacobson (2001) and Kirkevåg et al. (1999) show more generally that mixing of particles is important for the radiative effect of aerosols. In this study we will investigate internal mixing of sulfate aerosols with sea salt, mineral dust, and soot. In the latter case we will investigate different ways of internal mixing. We have assumed that sulfate is completely internally mixed with other aerosols. The following results must thus be regarded as sensitivity calculations as this assumption is not realistic. Observations show that sulfate and soot occur in a combination of externally and internally mixed states that varies with size (Naoe and Okada 2001; Okada and Hitzenberger 2001). Radiative forcing of external mixture of two aerosol components is found to be very similar to separate calculations for the aerosols (Myhre et al. 1998).

In the calculation assuming internal mixing of sulfate and soot we are in this study focusing on the impact of change in the radiative forcing due to sulfate and not the combined effect of soot and sulfate (as in Myhre et al. 1998). Therefore, our calculation assumes a fixed soot abundance. In this sensitivity experiment we adopt a mass

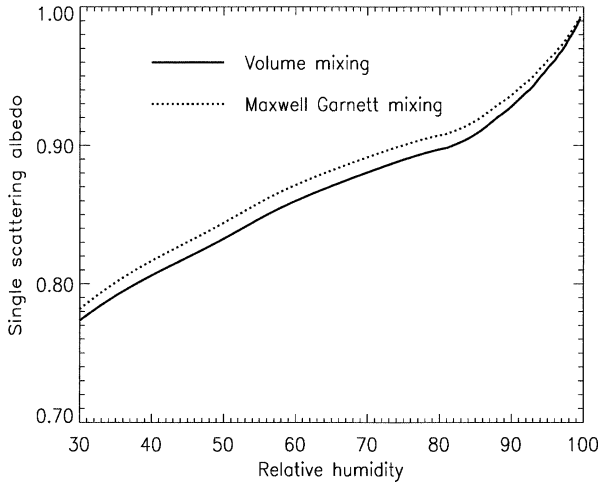

FIG. 7. Single scattering albedo at 550 nm as a function of relative humidity for internal mixing of sulfate and soot with volume mixing and the Maxwell–Garnett mixing.

fraction of soot of 0.075, compared to sulfate (as in Haywood et al. 1997b; Myhre et al. 1998). This assumption of mass fraction is clearly not realistic on a regional scale, but seems more reasonable on a global basis (Houghton et al. 2001) given the large uncertainty in modeling of the aerosol distribution. We investigate two types of mixing rules of the refractive indices of soot and sulfate (Chýlek et al. 1988); the standard volume mixing ratio approach and the Maxwell–Garnett mixing rule, which gives more realistic results for inhomogeneous mixing. Figure 7 shows the single scattering albedo at 550 nm for the two mixing rules. It demonstrates that the Maxwell–Garnett mixing rule yields higher values. The forcing due to sulfate is reduced substantially in these experiments with global and annual mean of -0.06 and -0.09 W m^{-2}, respectively. Figure 8b shows the distribution of the radiative forcing for the former case. Over regions with high surface albedo or large cloud cover, the radiative forcing is positive.

Internal mixing of sulfate aerosols with sea salt reduces the radiative forcing due to sulfate substantially over ocean. This can be seen by comparing Figs. 8c and 8d. This reduction in forcing is confined to oceanic and coastal regions. Particularly evident is the reduction in eastern North America, southern Europe, and eastern Asia. The spatial distribution and size distribution of sea salt are adopted from Koepke et al. (1997) and Hess et al. (1998), respectively. In Hess et al. (1998) a two-mode lognormal size distribution is given. The hygroscopic behavior for NaCl with parameterization from Fitzgerald (1975) is used. The calculations are performed only for one day in January, April, July, and October since very time-consuming interactive Mie calculations are performed. Such calculations are necessary as the sea salt (with varying size distributions) and sulfate concentrations vary in addition to the relative humidity. Interactive Mie calculations will probably be more important in the future when microphysical aerosol packages will be included in global transport models; alternatively, the simpler and parameterized approach in Ghan et al. (2001b) can be considered. Internal mixing of sulfate aerosols with sea salt increases the size of sulfate aerosols and therefore reduces their interaction with solar radiation. It is worth noticing that this simulation is strongly related to the calculation performed in section 3c(1), adopting observed aerosol size distributions over ocean.

For mixing of sulfate with mineral dust we have used a similar procedure as for mixing with sea salt, regarding source of data of the spatial distribution of mineral dust, aerosol size distribution, and optical calculations. The forcing due to sulfate is strongly reduced for an internal mixing with mineral dust, both over ocean and land (as can be seen by comparing Figs. 8c and 8e). Over the Arabian desert this reduction is particularly evident as the radiative forcing in the reference case is significant in this area. However, the forcing is reduced also around the Saharan desert, western North America, and eastern Asia. The reduction arises from the larger size of the mineral dust aerosols compared to sulfate aerosols (as for sea salt) and also from the absorbing properties of mineral dust (that are very uncertain), which reduces the scattering effect of the sulfate aerosols. The magnitude of the global mean reduction in the radiative forcing due to sulfate assuming internal mixing with sea salt and mineral dust, respectively, are relatively similar in these simulations. However, these simulations are very dependent on the spatial distribution of sulfate, sea salt, and mineral dust.

d. Meteorological data

1) SURFACE ALBEDO

In the reference calculation a broadband albedo neglecting any solar zenith angle dependence is assumed. Simulations where the surface albedo is modeled as function of solar zenith angle and wavelength have been performed. Over ocean, the surface albedo dependence on solar zenith angle is modeled as in Myhre et al. (2003), whereas over land, as in Briegleb et al. (1986). Surface albedo over land is based on vegetation data from Ramankutty and Foley (1999), with spectral distribution from Briegleb et al. (1986). The global mean radiative forcing due to sulfate aerosols changes only modestly, by 5%, compared to the reference case. The change is mainly due to inclusion of spectrally dependent surface albedo values and only to a small extent inclusion of solar zenith dependence. Over ocean, the forcing is almost unchanged, but over land regional differences up to 20%–25% occur (see Fig. 1j for geographical distribution in the forcing). For the global mean radiative forcing, the difference between the broadband surface albedo from ECMWF, on one hand, and the broadband values from Briegleb et al. (1986)

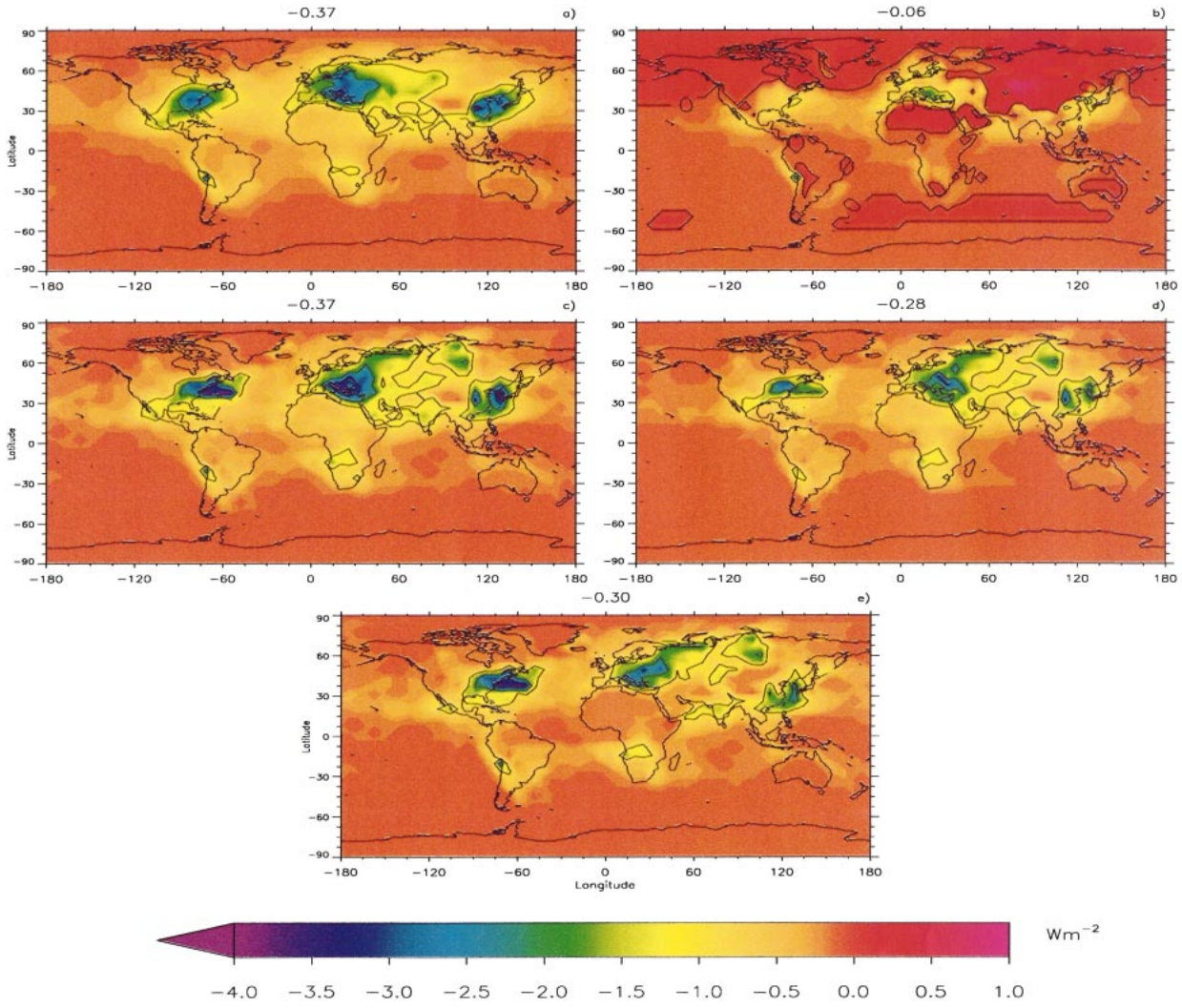

FIG. 8. Radiative forcing due to anthropogenic sulfate: (a) reference case (as shown in Fig. 1a); (b) internal mixing with soot; (c) reference case, but only for 4 days; (d) internal mixing with sea salt for 4 days; (e) internal mixing with mineral dust for 4 days.

and vegetation data from Ramankutty and Foley (1999), on the other hand, is less than 1%.

2) CLOUDS

Monthly mean cloud data (cloud cover, cloud optical depth, and cloud altitude) from the International Satellite Cloud Climatology Project (ISCCP; Rossow and Schiffer 1991) have been implemented in the radiative transfer calculations in a sensitivity study. The radiative forcing due to sulfate aerosols strengthens by about 15% compared to the reference case using ECMWF cloud data (see Fig. 1k for global distribution). A 3% difference in radiative forcing stems from the fact that monthly mean cloud data are used in the sensitivity study. The cloud radiative forcing in the reference calculation is -45 W m^{-2}, close to observed values (Ramanathan et al. 1989). The cloud radiative forcing using ISCCP cloud data is -31 W m^{-2}, which is in the weaker range of earlier estimates. In our two different calculations we have therefore probably covered most of the uncertainty range for the cloud radiative forcing.

3) RELATIVE HUMIDITY

Houghton et al. (2001) states that relative humidity is a major reason for the large range in previous global estimates of radiative forcing due to sulfate aerosols. This is owing to the different spatial and temporal resolutions used in the different models, as can be seen from the section regarding subgrid-scale variability in relative humidity. In the following, we will show that it is even more important that the relative humidity differs substantially between various models. We have tested four datasets for relative humidity in addition to the one used in the reference calculation. The National Cen-

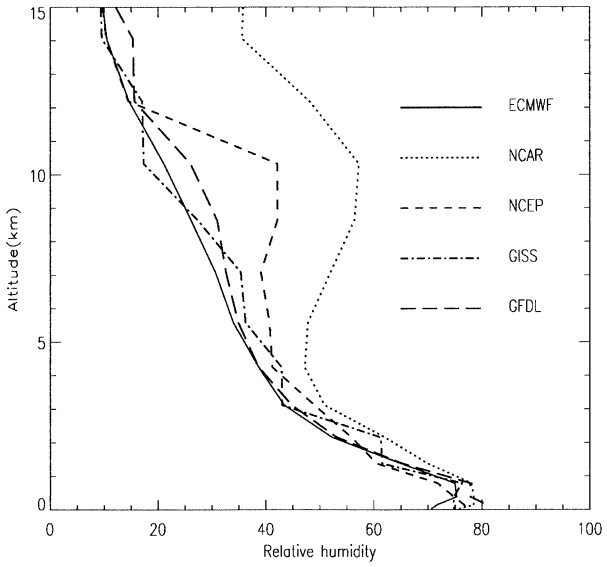

FIG. 9. Relative humidity as a function of altitude for five different datasets used in calculations in this study.

ter for Atmospheric Research (NCAR) Community Climate Model (CCM3; Kiehl et al. 1996) relative humidity is based on a 1-yr calculation representing current climate (L. Gulstad 2001, personal communication) with a 3-h resolution in relative humidity as in the reference dataset. The National Centers for Environmental Prediction (NCEP) analysis has a 4-h resolution in relative humidity and is for 1996 as in the reference calculation. The NCEP data are given up to 300 hPa, and we have used the ECMWF humidities above this altitude. The relative humidities from the Goddard Institute for Space Studies (GISS; Hansen et al. 1988) and the Geophysical Fluid Dynamics Laboratory (GFDL) (Delworth et al. 2002) global climate models (GCM) have 3-h and 24-h resolution, respectively.

Figure 9 shows the global and annual mean vertical profiles of the relative humidities for the five datasets. Noticeable and important differences in relative humidity in the lowest few kilometers can be seen. In the upper troposphere, the differences in relative humidities are larger, but as the sulfate concentration is much lower here and the sensitivity of forcing to relative humidity is lower at lower relative humidity, this is of much less importance for the radiative effect of sulfate aerosols. Figures 10a and 10b show the annual mean relative humidity for the five datasets in the lowest level in our model (about 60 m) and at about 1 km, respectively. Although the patterns in the five datasets appear to be similar, there are significant differences in the general relative humidity levels as well as the spatial distributions. The difference in relative humidity can easily be seen over ocean. However, more important for the radiative forcing due to sulfate aerosols are the differences over North America, Europe, and Southeast Asia. The global and annual mean GFDL relative humidities are highest of the five datasets near the surface, but at about 1 km, the NCAR data are highest. Large changes also occur for the other datasets between the surface and 1 km.

The differences in relative humidity introduce a large variation in the radiative forcing and its geographical distribution. The radiative forcing due to sulfate with relative humidities from NCAR, NCEP, GISS, and GFDL are shown in Figs. 1l–lo, respectively. The global mean radiative forcing due to sulfate using the NCAR relative humidities increases by 60% compared to the reference calculation with ECMWF humidities. For the three other datasets, the global mean radiative forcing is between the values based on NCAR and ECMWF. Regionally the NCAR relative humidities result in particularly strong forcing at high latitudes, but the forcing is also nearly twice as strong in some regions over Europe, North America, and Southeast Asia as in the reference case. With the GISS relative humidities the radiative forcing is particularly strong over Southeast Asia. With the GFDL data, this is the case over Europe.

To illustrate the differences in relative humidity between the datasets that introduce such a large effect on the forcing, Fig. 11 shows the percentage of grid points for the 10 lowest layers during the year with relative humidity above 80%, 90%, and 95%, respectively. The NCAR dataset has a larger fraction of high relative humidity than the other models. The fraction of relative humidities above 95% is especially important. The NCEP data yield a forcing, which is very similar to the reference case. This dataset has a higher fraction of relative humidities above 80% and 90% compared to the reference dataset. However, above 95% it has a rather similar fraction which is lower than for the three other datasets.

4. Summary

The aim of this study has been to explain the large range in earlier estimates of the radiative forcing due to sulfate aerosols. Houghton et al. (2001) assessed the range to be from -0.26 to -0.82 W m^{-2} in previous global estimates. The normalized radiative forcing has an even larger range (over a factor 4) from -110 to -460 W g^{-1}, indicating that the radiative effects of sulfate aerosols are quite uncertain. The tools we have used to explore the uncertainties in the radiative forcing due to sulfate aerosols are a CTM, including interactive chemistry to derive the sulfate distribution; Mie theory to determine the optical properties; and a radiative transfer model. In addition, we have used a wide range of datasets in various sensitivity calculations. We have concentrated on uncertainties involved in the optical properties and radiative transfer calculations.

One factor stands out as a major reason for the large spread in results, namely, the relative humidity. This is to some extent related to differences in temporal and spatial resolution, but mainly to differences in the level

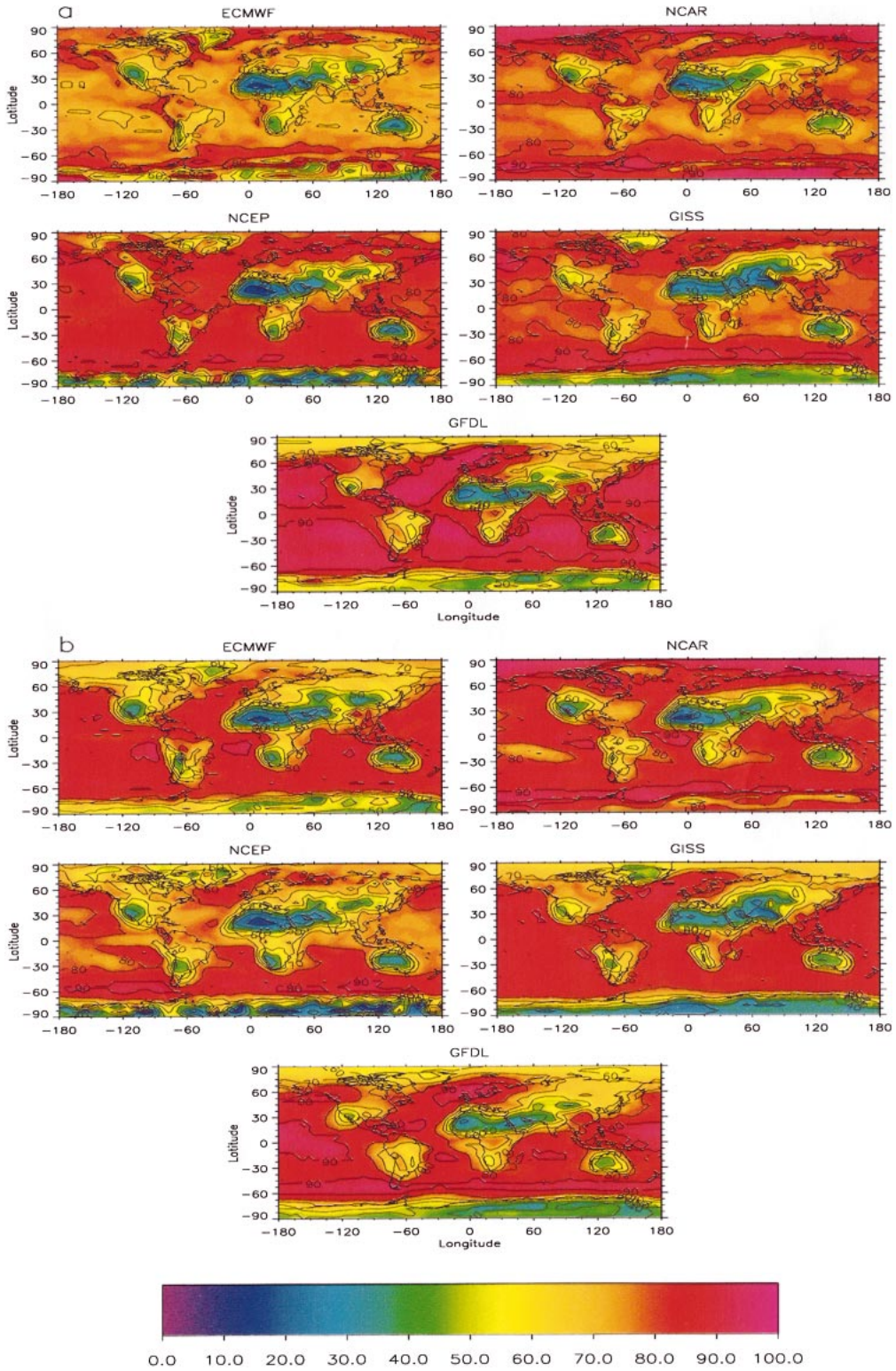

FIG. 10. Annual mean geographical distribution of the relative humidity at (a) the lowest layer in the model and (b) about 1 km.

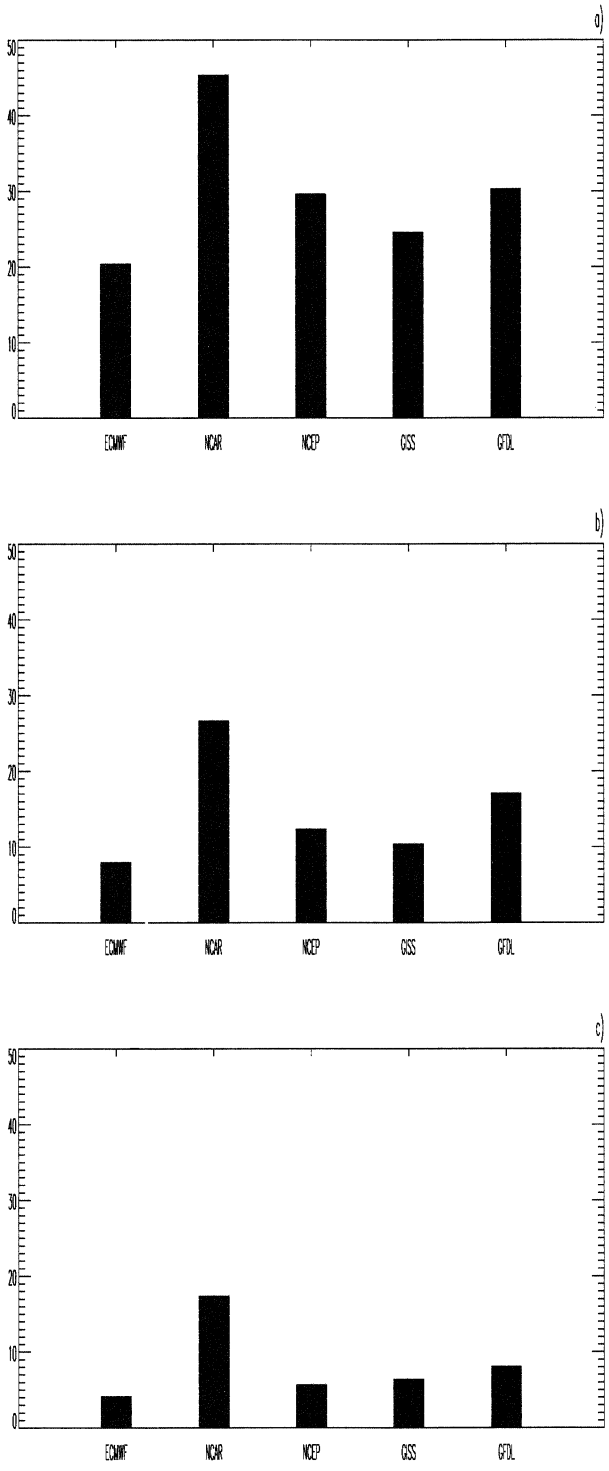

FIG. 11. Fraction of grid points below about 8 km with relative humidity above threshold values (a) 80%, (b) 90%, and (c) 95% for the ECMWF, NCAR, NCEP, GISS, and GFDL datasets.

and distribution of relative humidities. Using a different relative humidity field, from the NCAR CCM3, strengthened the radiative forcing due to sulfate by 60% compared to our reference case, which is based upon relative humidities from ECMWF. Earlier studies also may not have taken into account the growth of sulfate aerosols above certain threshold values, missing the large hygroscopic effect above 90% relative humidity. As long as the high relative humidities are taken into account, it seems not very sensitive to the particular parameterization. In a sensitivity study we used subgrid-scale information from a regional model with 50-km resolution and estimated a 15% strengthening in the radiative forcing. None of the previous global estimates have been performed with such a high spatial resolution. This effect has therefore not contributed to the large range in earlier estimates. The forcing due to sulfate can be even stronger owing to subgrid variability at higher resolutions than 50 km.

Another major reason for the large spread in the earlier results, and shown here as well, is the various assumptions made on mixing with other particles. Mixing influences the size distribution and the refractive indexes, which both strongly control the forcing. A relatively small change in the size distribution can easily change the forcing by 15%. This sensitivity to size is also pointed out in Charlson et al. (1999). Many of the earlier estimates have used size distributions similar to what we use in our reference case, but not all. A few earlier studies have included some absorption in the investigation of sulfate aerosols to take into account mixing with other particles, reducing the forcing. Earlier studies and simulations in this study show that mixing with soot substantially reduces the radiative impact of the sulfate aerosols. Mixing with sea salt and mineral dust also has the potential to reduce the radiative effect of sulfate aerosols, in this case more related to size than the refractive indexes. Observations show that the degree of mixing varies substantially in the real atmosphere.

One additional simulation was performed to illustrate the uncertainty associated with internal mixing and the relative humidity. In the calculation of internal mixing of sulfate and soot with relative humidity from ECMWF, the radiative forcing due to anthropogenic sulfate was -0.06 W m^{-2} [section 3c(6)]. A similar simulation, but with relative humidity from NCAR instead of ECMWF resulted in a radiative forcing due to sulfate of -0.29 W m^{-2}. This illustrates that uncertainties in the relative humidity may be even more important for the radiative effect of hygroscopic aerosols, which includes absorption, than for pure scattering aerosols.

Clouds reduce the radiative forcing due to sulfate aerosols. The uncertainty in this effect is substantial (Houghton et al. 2001). In addition to this uncertainty in radiative forcing in cloudy regions, clouds contribute to uncertainties in radiative forcing by the fact that the forcing depends on collocation of clouds and relative

humidity, which is not perfectly reproduced in models. However, simulations in this study using ISCCP cloud data instead of ECMWF data did not result in major differences. The radiative effect of clouds are very different for the two datasets adopted. In addition the ISCCP data represent an average over the 1984 to 1990 period, whereas ECMWF data represent a specific year, so the spatial distribution is also different. For the radiative effect due to biomass burning aerosols in southern Africa, it was found that dependence of surface albedo on wavelength and solar zenith angle strengthened the forcing substantially (Myhre et al. 2003). However, on a global scale this is not the case for sulfate aerosols, mainly owing to the constant single scattering albedo for sulfate below 2 μm. We find also only small differences in the forcing when we use two independent surface albedo datasets.

In summary, the range of earlier estimates of radiative forcing due to sulfate aerosols seems to arise from a wide range of sources. Many of these are connected to the hygroscopic growth of the sulfate aerosols and therefore the relative humidity. Some of these are linked directly to assumptions regarding the hygroscopic growth but also to different spatial and temporal (some have used monthly mean) resolution of relative humidity. Finally, there are large variations in various datasets for relative humidity used in calculations of radiative forcing due to sulfate aerosols originating from different models or reanalyses.

Clouds and aerosol optical properties are other factors contributing to the uncertainty. Boucher et al. (1998) found relatively small differences (up to 20%) between the various radiative transfer schemes used for calculation of the radiative effect of sulfate aerosols, but this still contributes to the overall uncertainty. Finally, the sulfate distribution itself is a major source to the large range as the sulfate spatial distribution is very important. In Myhre et al. (1998) it was shown that the radiative forcing due to sulfate aerosols was generally much stronger over ocean than land and much stronger at low latitudes than at high latitudes for a constant sulfate change. The vertical distribution is also important as the vertical variation in relative humidity is strong. Haywood and Ramaswamy (1998) found a 30% difference in the normalized forcing due to a difference between two sulfate distributions, which they ascribe mostly to differences in the vertical profile. However, in this study we find relatively small differences in the normalized radiative forcing for three sulfate distributions, despite large variation in the geographical distribution of sulfate. Further, the Langner and Rodhe (1991) sulfate distribution is more constant vertically in the lowest 1 km, and thereafter more strongly decreasing with altitude compared to the reference calculation.

To reduce the large uncertainties in the radiative forcing due to sulfate aerosols, it is necessary to improve relative humidities in the models. Special efforts are needed to investigate variation in the relative humidity variation at high spatial resolution. Another critical point is mixing of aerosols. Observations are needed to understand and quantify aerosols mixing, both in situ measurements and satellite remote sensing.

Acknowledgments. This work has been supported by the Research Council of Norway, through the RegClim project.

REFERENCES

Adams, P. J., J. H. Seinfeld, D. Koch, L. Mickley, and D. Jacob, 2001: General circulation model assessment of direct radiative forcing by sulfate-nitrate-ammonium-water inorganic aerosol system. *J. Geophys. Res.*, **106,** 1097–1111.

Berntsen, T., and I. S. A. Isaksen, 1997: A global three-dimensional chemical transport model for the troposphere, 1, Model description and CO and ozone results. *J. Geophys. Res.*, **102,** 21 239–21 280.

Boucher, O., 1998: On the aerosol direct shortwave forcing and the Henyey–Greenstein phase function. *J. Atmos. Sci.*, **55,** 128–134.

——, and T. L. Anderson, 1995: GCM assessment of the sensitivity of direct climate forcing by anthropogenic sulfate aerosols to aerosol size and chemistry. *J. Geophys. Res.*, **100,** 26 117–26 134.

——, and Coauthors, 1998: Intercomparison of models representing direct shortwave radiative forcing by sulfate aerosols. *J. Geophys. Res.*, **103,** 16 979–16 998.

Briegleb, B. P., P. Minnis, V. Ramanathan, and E. Harrison, 1986: Comparison of regional clear-sky albedos inferred from satellite observations and models comparisons. *J. Climate Appl. Meteor.*, **25,** 214–226.

Charlson, R. J., J. Langner, H. Rodhe, C. B. Leovy, and S. G. Warren, 1991: Perturbation of the Northern Hemisphere radiative balance by backscattering from anthropogenic sulfate aerosols. *Tellus*, **43AB,** 152–163.

——, T. L. Anderson, and H. Rodhe, 1999: Direct climate forcing by anthropogenic aerosols: Quantifying the link between atmospheric sulfate and radiation. *Contrib. Atmos. Phys.*, **72,** 79–94.

Chylek, P., V. Srivastava, R. G. Pinnick, and R. T. Wang, 1988: Scattering of electomagnetic waves by composite spherical particles: Experiments and effective medium approximations. *Appl. Opt.*, **27,** 2396–2404.

Covert, D. S., and J. Heintzenberg, 1993: Size distributions and chemical properties of aerosol at Ny Ålesund, Svaldbard. *Atmos. Environ.*, **27A,** 2989–2997.

Delworth, T. L., R. J. Stouffer, K. W. Dixon, M. J. Spelman, T. R. Knutson, A. J. Broccoli, P. J. Kushner, and R. T. Wetherald, 2002: Review of simulations of climate variability and change with the GFDL R30 coupled climate model. *Climate Dyn.*, **19,** 555–574.

Fitzgerald, J. W., 1975: Approximation formulas for the equilibrium size of an aerosol particle as a function of its dry size and composition and ambient relative humidity. *J. Appl. Meteor.*, **14,** 1044–1049.

Ghan, S. J., and Coauthors, 2001a: A physically based estimate of radiative forcing by anthropogenic sulfate aerosol. *J. Geophys. Res.*, **106,** 5279–5293.

——, N. Laulainen, R. Easter, R. Wagener, S. Nemesure, E. Chapman, Y. Zhang, and R. Leung, 2001b: Evaluation of aerosol direct radiative forcing in MIRAGE. *J. Geophys. Res.*, **106,** 5295–5316.

Hansen, J., I. Fung, A. Lacis, D. Rind, S. Lebedeff, R. Ruedy, G. Russel, and P. Stone, 1988: Global climate changes as forecast by Goddard Institute for Space Studies: Three-dimensional model. *J. Geophys. Res.*, **93,** 9341–9364.

Haywood, J. M., and V. Ramaswamy, 1998: Investigations into the direct radiative forcing due to anthropogenic sulfate and black carbon aerosol. *J. Geophys. Res.*, **103,** 6043–6058.

——, and O. Boucher, 2000: Estimates of the direct and indirect radiative forcing due to tropospheric aerosols: A review. *Rev. Geophys.*, **38,** 513–543.

——, V. Ramaswamy, and L. J. Donner, 1997a: A limited-area-model case study of the effects of sub-grid scale variations in relative humidity and cloud upon the direct radiative forcing of sulfate aerosol. *Geophys. Res. Lett.*, **24,** 143–146.

——, D. L. Roberts, A. Slingo, J. M. Edwards, and K. P. Shine, 1997b: General circulation model calculations of the direct radiative forcing by anthropogenic sulfate and fossil-fuel soot aerosol. *J. Climate*, **10,** 1562–1577.

Hess, M., P. Koepke, and I. Schult, 1998: Optical properties of aerosols and clouds: The software package OPAC. *Bull. Amer. Meteor. Soc.*, **79,** 831–844.

Hesstvedt, E., Ø. Hov, and I. S. A. Isaksen, 1978: Quasi steady-state approximation in air pollution modelling: Comparison of two numerical schemes for oxidant prediction. *Int. J. Chem. Kinet.*, **10,** 971–994.

Hogan, R. J., and A. J. Illingworth, 2000: Deriving cloud overlap statistics from radar. *Quart. J. Roy. Meteor. Soc.*, **126,** 2903–2909.

Holtslag, A. A. M., E. I. F. De Bruijn, and H.-L. Fan, 1990: A high resolution air mass transformation model for short-range weather forecasting. *Mon. Wea. Rev.*, **118,** 1561–1575.

Houghton, J. T., Y. Ding, D. J. Griggs, M. Noguer, P. J. van der Linden, X. Dai, K. Maskell, and C. A. Johnson, Eds., 2001: *Climate Change 2001: The Scientific Basis.* Cambridge University Press, 98 pp.

Jacobson, M. Z., 2001: Global direct radiative forcing due to multicomponent anthropogenic and natural aerosols. *J. Geophys. Res.*, **106,** 1551–1568.

Kiehl, J. T., J. J. Hack, G. B. Bonan, B. A. Boville, B. P. Briegleb, D. L. Williamson, and P. J. Rasch, 1996: Description of the NCAR community climate model (CCM3). NCAR Tech. Note NCAR/TN-420+STR, 152 pp.

Kirkevåg, A., T. Iversen, and A. Dahlback, 1999: On radiative effects of black carbon and sulphate aerosols. *Atmos. Environ.*, **33,** 2621–2635.

Koepke, P., M. Hess, I. Schult, and E. P. Shettle, 1997: Global aerosol data set. Max Planck Institute for Meteorology Tech. Rep. 243, Hamburg, Germany, 44 pp.

Langner, L., and H. Rodhe, 1991: A global three-dimensional model of the tropospheric sulfur cycle. *J. Atmos. Chem.*, **13,** 225–263.

Myhre, G., F. Stordal, K. Restad, and I. S. A. Isaksen, 1998: Estimation of the direct radiative forcing due to sulfate and soot aerosols. *Tellus*, **50B,** 463–477.

——, J. E. Jonson, J. Bartnicki, F. Stordal, and K. P. Shine, 2002: Role of spatial and temporal variations in the computation of radiative forcing due to sulphate aerosols: A regional study. *Quart. J. Roy. Meteor. Soc.*, **128,** 973–989.

——, T. K. Berntsen, J. M. Haywood, J. K. Sundet, B. N. Holben, M. Johnsrud, and F. Stordal, 2003: Modeling the solar radiative impact of aerosols from biomass burning during the Southern African Regional Science Initiative (SAFARI-2000) experiment. *J. Geophys. Res.*, **108**, 8501, doi:10.1029/2002JD002313.

Naoe, H., and K. Okada, 2001: Mixing properties of submicrometer aerosol particles in the urban atmosphere with regard to soot particles. *Atmos. Environ.*, **35,** 5765–5772.

Okada, K., and R. M. Hitzenberger, 2001: Mixing properties of individual submicrometer aerosol particles in Vienna. *Atmos. Environ.*, **35,** 5617–5628.

Palmer, K. F., and D. Williams, 1975: Optical constants of sulfuric acid: Application to the clouds of Venus. *Appl. Opt.*, **14,** 208–219.

Prather, M. J., 1986: Numerical advection by conservation of second-order moments. *J. Geophys. Res.*, **91,** 6671–6681.

Pruppacher, H. R., and J. D. Klett, 1978: *Microphysics of Clouds and Precipitation.* D. Reidel Publishing Company, 714 pp.

Quinn, P. K., S. F. Marshall, T. S. Bates, D. S. Covert, and V. N. Kapustin, 1995: Comparison of measured and calculated aerosol properties relevant to the direct radiative forcing of tropospheric sulfate aerosol on climate. *J. Geophys. Res.*, **100,** 8977–8991.

Ramanathan, V., R. D. Cess, E. F. Harrison, P. Minnis, B. R. Barkstrom, E. Ahmad, and D. Hartmann, 1989: Cloud-radiative forcing and climate: Results from the Earth Radiation Budget Experiment. *Science*, **243,** 57–63.

Ramankutty, N., and J. Foley, 1999: Estimating historical changes in global land cover: Cropland from 1700 to 1992. *Global Biogeochem. Cycles*, **13,** 997–1027.

Rossow, W. B., and R. A. Schiffer, 1991: ISCCP cloud data products. *Bull. Amer. Meteor. Soc.*, **72,** 2–20.

Slingo, A., 1989: A GCM parameterization for the shortwave radiative properties of water clouds. *J. Atmos. Sci.*, **46,** 1419–1427.

Stamnes, K., S.-C. Tsay, W. Wiscombe, and K. Jayaweera, 1988: A numerically stable algorithm for discrete-ordinate-method radiative transfer in multiple scattering and emitting layered media. *Appl. Opt.*, **27,** 2502–2509.

Stephens, G. L., and C. M. R. Platt, 1987: Aircraft observations of the radiative and microphysical properties of stratocumulus and cumulus cloud fields. *J. Climate Appl. Meteor.*, **26,** 1243–1269.

Tiedtke, M., 1989: A comprehensive mass flux scheme for cumulus parameterization on large scale models. *Mon. Wea. Rev.*, **117,** 1779–1800.

Toon, O. B., J. B. Pollack, and B. N. Khare, 1976: The optical constants of several atmospheric aerosol species: Ammonium sulphate, aluminium oxide and sodium chloride. *J. Geophys. Res.*, **81,** 5733–5748.

Weingartner, E., S. Nyeki, and U. Baltensperger, 1999: Seasonal and diurnal variation of aerosol size distribution ($10<D<750$ nm) at a high-alpine site (Jungfraujoch 3580 m asl). *J. Geophys. Res.*, **104,** 26 809–26 820.

Whitby, K. T., 1978: The physical characteristics of sulfur aerosols. *Atmos. Environ.*, **12,** 135–159.

Wiscombe, W., and J. Evans, 1977: Exponential-sum fitting of radiative transmission functions. *J. Comput. Phys.*, **24,** 416–444.